Feasibility Study of Medium-Power Helicon Thruster

D. Pavarin[1], M. Manente[2], Y. Guçlua[3], D. Curreli[3], C. Bettanini[2], M. Zaccariotto[2],
CISAS university of Padua 35131 Padova

M. Walker[4], D. Palmer[5]
Georgia Institute of Technology, Atlanta, GA, 30332, USA

J. Carlsson[6]
Tech-X corporation, Boulder CO USA

C. Bramanti[7]
Advanced Concept Team ESA ESTEC Noordwijk - The Netherlands

and E. Lorenzini[8]
Department of Mechanical Engineering University of Padua

A medium-power (1.5 kW) plasma thruster based on a helicon source is considered as a candidate for primary space propulsion. A high-density plasma is produced by the use of a radio frequency (RF) transmitting antenna, which produces helicon waves to ionize a neutral gas (*e.g.*, argon, krypton, xenon, helium or hydrogen) flowing through a tube and confined by a magnetic field. The plasma is accelerated through a potential drop created by a divergent magnetic field, giving a sudden reduction in electron density (and hence plasma potential) very close to the open end of the source tube. The plasma may then expand through a "magnetic nozzle" into the vacuum. Numerical studies are conducted by CISAS in order to investigate the physics connected with the potential drop. The analysis is conducted through a combination of 1-D and 2-D numerical codes. The PPDL code is developed and used for the 1-D analysis. The main features of the code are: hybrid Boltzmann electron/drift-kinetic ion, inclusion of dominant 2-D effects, and high computational efficiency thorough implicit non linear Boltzmann solver. The 2-D analysis is performed with XOOPIC, an open source code available from Berkeley University. The combined approach is very useful since the 1-D code is used to screen many different experimental conditions and to identify the correct boundary conditions. The 2-D code is then used to refine 1-D results. The two models, combined with a global model, specifically developed to simulate the plasma reaction inside the plasma source, are run through genetic algorithms to identify an optimal thruster configuration in the 1500-W power regime. In addition, the thruster is thermally and mechanically sized.

Nomenclature

A = cross surface of the cell revolution
A_{EXH} = geometrical exhaust area
BSCCO = Bismuth Strontium Calcium Copper Oxide

---

[1] Researcher, Department of Mechanical Engineering University of Padua Via Venezia 1 35131 Padua
[2] Post-doc fellow CISAS University of Padua Via Venezia 1535131 Padova Italy
[3] Ph.D. student CISAS University of Padua 35131Via Venezia 15 Padua Italy
[4] Assistant Professor, Aerospace Engineering, Georgia Institute of Technology, Atlanta, GA, 30332, USA
[5] Graduate Student Researcher, Aerospace Engineering, Georgia Institute of Technology, Atlanta, GA, 30332, USA
[6] Senior researcher, Tech-X corporation, 5621 Arapahoe Ave Suite A, Boulder, CO 80303
[7] ESA technical officer, Advanced Concept Team ESTEC - DG-PI, Keplerlaan 1 - 2201 AZ Noordwijk - The Netherlands
[8] Full professor Department of Mechanical Engineering University of Padua Via Venezia 1 35131 Padua

c_p = coefficient
c_s = coefficient
E_{THi} = Threshold energy for *i*-th reaction
e = electron charge
I_{sp} = specific impulse
K_i = reaction rate for *i*-th species
K_B = Boltzmann constant
L_{EXH} = ion loss at the exhaust
m = particle mass
m_{ion} = ion mass
n = plasma density
n_e = electron density
n_i = density of *i*-th species
n_j = density of the species involved in the *i*-th reaction
P_{ABS} = deposited power
P_{EXH} = power loss associated with the electron and ion flux at the exhaust
P_i = power lost in the *i*-th reaction
P_w = power lost at the exhaust
r = radius of magnetic lines tube
r_i = radius of the detachment cell
S/C = spacecraft
T = particle temperature
T_e = electron temperature
U_B = ion Bohm velocity
V_a = average axial velocity inside the detachment cell
V_e = plasma volume
Z = position
Γ_{EXH} = flux loss term due to the particle flow through the exhaust for the *i*-th species
Γ^l_i = flux loss term due to plasma processes for the *i*-th species
Γ^s_i = flux source term due to plasma processes for the *i*-th species
Γ_{Wi} = flux loss term due to particle recombination at wall for the *i*-th species
σ = cross section

I. Helicon Thruster Numerical Models

The proposed modeling approach is based on three numerical models 1) a global numerical model of the plasma source, 2) a 1-D PIC code of the entire system, and 3) a 2-D PIC code of the entire system. The global model is used to simulate the plasma source behavior. It provides the source ionization rate, plasma density, and electron temperature to the PPDL and XOOPIC codes. A 1-D code named PPDL is specifically developed for this purpose. It is a hybrid code with Boltzmann electrons and drift-kinetic ions. It includes dominant 2-D effects and high computational efficiency through implicit nonlinear Boltzmann solver. The 2-D code used is XOOPIC, freely available from University of California at Berkeley. XOOPIC performs fully electrostatic simulations with kinetic electrons, which results in long computational times in order to analyze detachment features. A combined approach proved very useful, where the 1-D code is used to rapidly screen many different experimental conditions and to identify the right boundary condition. The 2-D code is used to refine the 1-D results.

A. Plasma source numerical model

A global model to describe the plasma source is developed. This approach is similar to other global models from past studies.[5-10]. The plasma balance equations for particles and energy are written for uniformly distributed plasma inside of a region confined by a magnetic field. Many studies are carried out to understand the interactions between plasma and neutrals, including the effect of neutral losses to ionization[5-8,26,27] and neutral heating.[18-19] Several models take into account the neutral density by inserting a source term and a sink term into the neutrals balance equation.[5-9,12-17] These terms are related to the feeding flow from the reservoir and the flow to the vacuum pump. In other models, the plasma neutral interactions are not considered, and no equations are written to follow the neutral density behavior.[10,11] Due to the specific gas-dynamic configuration of the device, the neutral interaction with plasma is considered in this work by coupling a global gas-dynamic model of the entire system, with a global plasma model of the source. This model provides an estimate for the pop-off feeding-valve operation, efficiency of neutral pumping by the vacuum pump, and efficiency of a gas trap in the source to increase the ionization efficiency. The interactions that are taken into account in the model are:

- Neutral density reduction due to ionization;
- Neutral dissociation (molecular species-atom species);
- Global gas dynamic analysis behavior in the plasma source and in the vacuum chamber;
- Wall recombination and volume recombination in the main vacuum chamber.

Plasma is generated in the source chamber. A preliminary investigation shows that in specific magnetic field configurations or in a certain operation mode (helicon mode), the majority of the plasma could be confined inside of a volume smaller than the source chamber volume.[1]

We assume the plasma is confined in a cylindrical volume V_e of length L and radius r_p. Inside this volume different species are considered for every gas. The model follows the density of all of these species. Plasma flows and diffuses also through the external surfaces of the volume V_e. These surfaces will be named to highlight the different processes involved. The back axial surface is the surface in front of the feeding orifice. Plasma in this zone is electrostatically confined and the mass loss is calculated using Godyac and Maximov[25] solution of diffusion equation. Plasma also diffuses through the radial surface, but in this zone the magnetic field generated by the solenoid coil improves the confinement. The particle loss in this area is calculated using again the Godyac and Maximov solution modified by Cheetham[10] to take into account the magnetic field contribution to the confinement. The radial surface toward the vacuum chamber is named the exhaust surface. Plasma flows in this zone with a speed that is a fraction of the ion sound velocity. The speed depends strongly on the shape of the plasma potential in this area. This calculation is beyond the purpose of this model, so a parameter is introduced into the numerical analysis named c_s. Thus, the exhaust velocity is the ion sound velocity multiplied by the c_s coefficient that is considered as a free parameter. Particles that diffuse through the lateral surface and through the back axial surface are neutralized.

The plasma equations are coupled with neutral equations since in the source chamber the neutrals density is not constant, but free to change in relation to the neutral flow, the dissociation processes and the plasma-neutral interaction. The reactions that involve ionized species and electrons are found in literature.[23,28] The particle balance equations for the ionized particles and electrons are written in a particle flux form, (particles/m^3/s). The general form for the balance equations of charged particles is:

$$\frac{dn_i}{dt} = \Gamma_i^s - \Gamma_i^l - \Gamma_{Wi} - \Gamma_{EXH-i} \tag{1}$$

where Γ_i^s is for the i-species the source term due to plasma processes, Γ_i^L is the loss term due to plasma processes, Γ_{Wi} is for the i-species the loss term due to particle recombination at the wall (the particle diffuses through the wall sheath before reaching the wall), Γ_{EXH} is the loss term due to the particle flow through the exhaust. The reaction rates are obtained averaging the cross section for the specific reaction over a Maxwellian distribution[28]

$$K_i = \left(\frac{m}{2\pi kT}\right)^{3/2} \int_0^\infty \sigma(v) v \exp\left(-\frac{mv^2}{2kT}\right) 4\pi v^2 dv \tag{2}$$

where T is the electron temperature in eV and m is the particle mass and σ the cross section. Wall losses are calculated as in References 16, 19, 26-27, and 19. Ions lost at the exhaust are calculated as:

$$\begin{aligned} L_{EXH} &= n_i \cdot u_B \cdot A_{EXH} \cdot cp \\ u_B &= \sqrt{\frac{kT_e}{m_i}} \end{aligned} \tag{3}$$

where u_B term is the ion Bohm velocity and A_{EXH} is the geometrical exhaust area.

The exhaust flow is affected by the magnetic field at the exit of the plasma discharge section. At the exit of the plasma discharge section the magnetic field increases and then decreases. This peak acts as a magnetic mirror that reflects part of the plasma flow. Therefore, the net flow is given by the difference between the incident flow and the reflected flow. The reflected flow depends on the configuration of the magnetic field and on the plasma parameters.

The power balance equation is written as follows (units: W/m^3)

$$\frac{P_{ABS}}{Ve} = \frac{d}{dt}\left(\frac{3}{2}\cdot e \cdot n_e \cdot T_e\right) + \sum P_i + P_W + P_{EXH} \tag{4}$$

where P_{ABS} is the deposited power into the plasma that is assumed to be known. e is the electron charge, T_e is the electron temperature, V_e again the plasma volume. P_i terms are the power lost in the *i*-reaction. The general formula is:

$$P_i = K_i \times E_{TH\text{-}i} \times n_e \times n_j \tag{5}$$

where K_i is the rate constant for the specific reaction, $E_{TH\text{-}i}$ the threshold energy for the i-reaction[23], n_e the electron density, n_j the density of the species involved in the i-reaction. P_W is the power lost at the wall due to the electron-ions flow. P_{EXH} is the power loss associated with the electron and the ion flux at the exhaust, assuming that the escaping velocity is the ion-Bohm velocity. Experimental results[33] indicate the presence of a hot tail in the electron population in hydrogen and helium discharge. This distribution is modeled summing two Maxwellian distributions: one with the temperature of the bulk of the plasma and one with the temperature of the hot tail. The power balance can be used to solve for the electron temperature.

B. 1-D PIC Numerical model

The PPDL is a modified version of an existing 1-D PIC named PadPIC, a Particle in Cell[35,43] plasma simulator. The main features of PPDL are:

- Drift-kinetic ions, where the magnetic moment is assumed to be an adiabatic invariant. The drift-kinetic equation of motion includes the ΔB force from the expanding magnetic field,
- Expansion of the magnetic field is considered,
- Boltzmann electrons, assuming Maxwellian distribution and inertialess,
- Floating boundary conditions, and
- Plasma generation is simulated through a source term.

The advantage of Boltzmann electrons is that electron time scale (plasma and gyro periods) do not have to be resolved. Nonetheless, it requires a non-linear Poison solver to determine the electrostatic potential. With the hybrid Boltzmann electron/drift-kinetic ion approach, the time step is only limited by ion period, which is two orders of magnitude larger than electron plasma period and ion gyro period, which can become very short in a strong magnetic field. Thus, PPDL is very fast, efficient, and still capable of simulating the relevant physics. To better fit the experimental set-up, the presence of magnetic field is simulated by the analytic solution of a field generated by one or more solenoids. The gradient of the magnetic field is also calculated analytically and used for adding the ∇B velocity to the drift-kinetic ions. The dilution of the charge density due to the expanding magnetic field has also been incorporated into the non linear Poisson solver.

We consider a plasma of radius r_0, density n_0, and temperature T_e created in a uniform field B_0 and then inject it into a region of expanding field lines. The model assumes that the plasma is frozen to the field lines. Thus, the field $B(z)$ and the density $n(z)$ in the expansion region are related to the plasma radius as:

$$\frac{n}{n_0} = \frac{B}{B_0} = \left(\frac{r_0}{r}\right)^2 \tag{6}$$

where $r(z)$ is the radius of magnetic lines at position *z*.

C. 2-D OOPIC Numerical model

As previously mentioned, the code used for the 2-D simulation is the OOPIC (Object-Oriented Particle-In-Cell) (or XOOPIC, which has a GUI). OOPIC is a 2D-3V relativistic electromagnetic PIC code. The object-oriented paradigm provides the opportunity for advanced PIC modeling, increased flexibility, extensibility and efficiency.[34] OOPIC includes a 2-D orthogonal grid: Cartesian (x,y) or cylindrically symmetric (r,z) moving window, electrostatic and electromagnetic fields, and relativistic particles. The boundaries are determined at runtime and include many models of emitters, collectors, wave boundary conditions and equipotentials. Because the dependence on the azimuthal angle is not expected to be relevant for DL experiments, we use a 2D *r-z* cylindrical PIC simulation. The code can handle an arbitrary number of species, particles, and boundaries. The code also includes Monte Carlo collision (MCC) algorithms for modeling collisions of charged particles with a variety of neutral background gasses. Figure 1 presents the geometry configuration used for the simulations.

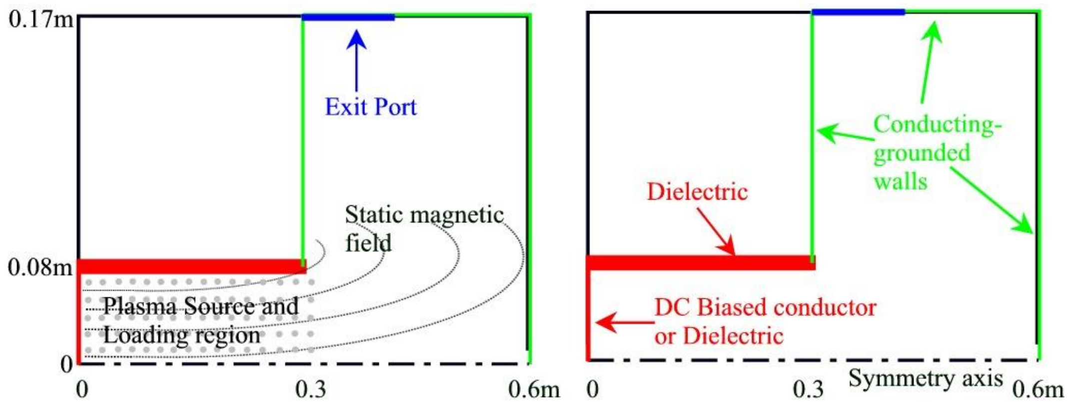

Figure 1 - Geometry configuration used for XOOPIC simulation

A detailed model of the helicon source is not our intention. The reproduction of its heating process is avoided by imposing ad hoc electron and ions families, emerging from the source tube. This is a versatile approach because it is possible to change the parameters, thus simulating plasma expansion in different conditions. The resolution of the particles motion is done under the electrostatic assumption. Few particles are immediately loaded into the source region, to represent the high energy electrons produced during the breakdown and to start without an empty region, while most are created during the simulation. The plasma production is represented by the OOPIC Plasma Source object. The particles are created at a given rate in a rectangular area and with Maxwellian velocity distribution and a changeable density distribution. Figure 2 shows the plasma production density, which is defined in order to model the typical helicon source behavior: maximum density near r=0 and after the tube half. The static magnetic field is calculated by solving the equations for circular filamentary coils in 2-D. Two, 8-cm long solenoids are located around the source tube (r=12-13 cm) at axial positions of 1 and 20 cm.

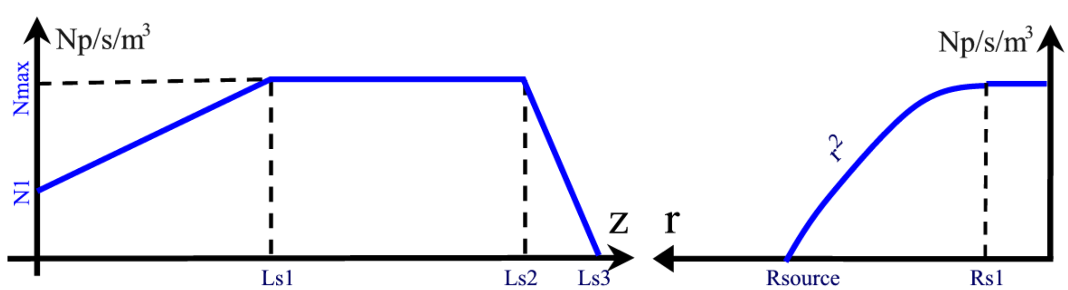

Figure 2 - Plasma production density distribution: Ls3=Lsource=30cm, Rs1=1.5cm and N1=Nmax/3

II. Thrust Performance Evaluation

The thrust is calculated with OOPIC for four different detachment lines. The selection of these lines considers the axial positions from which the direction of the ion velocity starts to be constant. It is assumed that the detachment distance from the helicon tube exit grows with the axial position. Figure 3 shows the ion and electron trajectories. The detachment distance is greater than 20 cm at the tube axis and nearly constant, but more than 60 cm for r greater than 30 cm. The equation $T=\sum m\, N\, V_a^2 A$ is iterated for every r_i along the supposed detachment line, where m is the ion mass, N is the density of ions inside the detachment cell at radius r_i, V_a is the average axial velocity inside the detachment cell, and A is the cross area of the cell revolution along φ, $A=\pi[(r_i+dr)^2-r_i^2]$. Therefore, for all the cells that follow the selected line we have evaluated the ion density, which is a default output of OOPIC, and the average ion axial velocity. The result is a thrust between $1\text{x}10^{-9}$ N and $7\text{x}10^{-9}$ N. This is obtained by comparing three simulations made with T_e=8 eV, 70 V DC biased left wall and diffusion chambers 1m long with different electrical properties. The simulations predict a density inside the source tube of approximately 5 x 10^{13} m^{-3}, where the source rate is set between 10^{18} and 3 x 10^{18} m^{-3} s^{-1}. The specific impulse (I_{sp}) can be evaluated through the formula $I_{sp}=(\sum N\ V_a)/(\ \sum N\ g)$, iterated again along the supposed detachment line and where g is the gravitational acceleration.

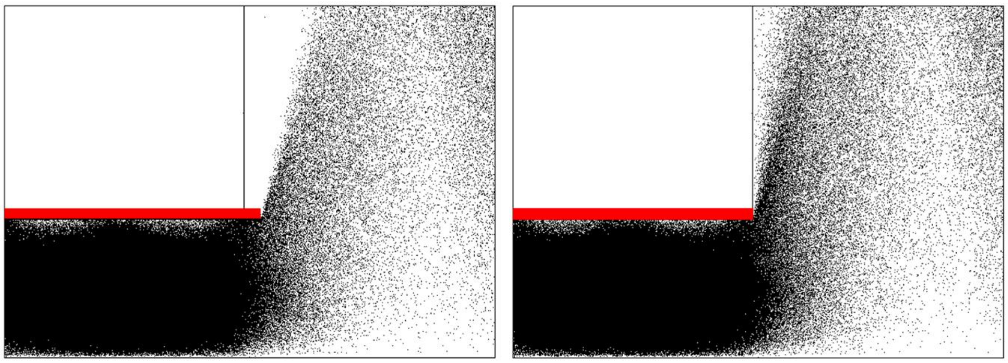

Figure 3 - Ion right) and electron left) trajectory at the thruster exhaust.

III. Thruster Design

The thruster is designed through the combination of numerical simulations and a genetic optimization algorithm. The models described above are combined with a lumped structural model, which provides the total volume and mass of the device, depending on the selected thruster configuration (*i. e.*, mass flow, magnetic field, power, etc.). A genetic optimization algorithm is then used to identify the best thruster configuration, trading off among performance, weight, and volume. The global model is combined with the structural model to identify the most promising configuration. All configurations are analyzed with the 1-D PIC model in order to identify three best. These configurations are then investigated with the 2-D PIC code in order to evaluate thrust and I_{sp}. The power is fixed at 1500 W, and the magnetic field is fixed at 1000 Gauss in order to allow very compact thruster, keeping the Larmor radius compatible with the thruster size. The genetic optimization algorithm identifies as best trade-off among high I_{sp} and thrust for the parameters in Table 1.

Table 1 – Thruster Specifications

Source diameter	25 mm
Source length	70 mm
Mass flow rate	0.05 kg/s

Figure 5 shows the variation of electron density, electron temperature, specific impulse and thrust with mass flow rate. As expected, an increase in mass flow rate increases the electron number density, but reduces electron temperature and thus I_{sp}.

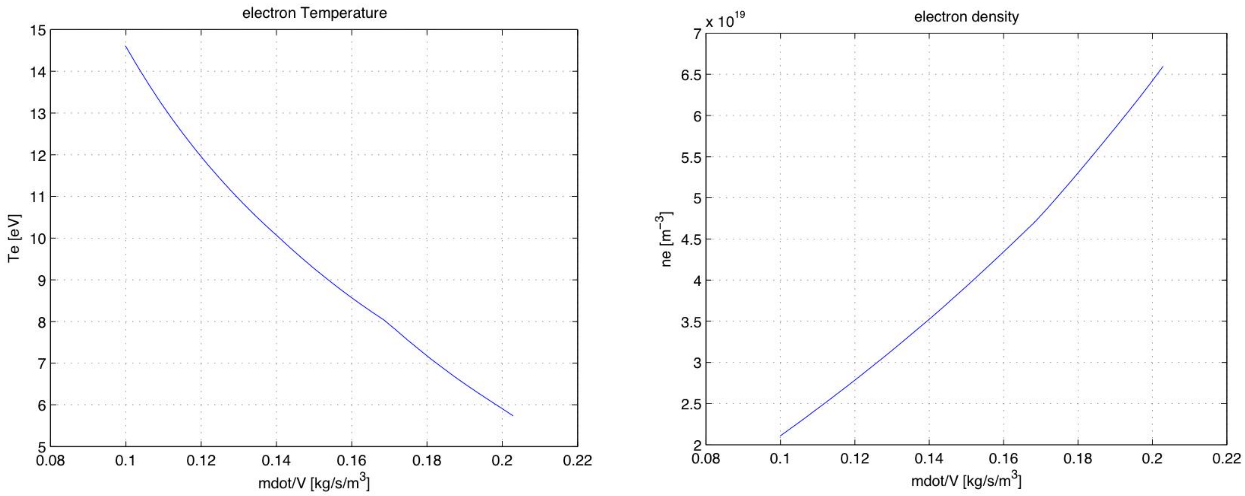

Figure 4 - Electron temperature, electron density, and neutral density versus mass flow rate normalized by the source volume.

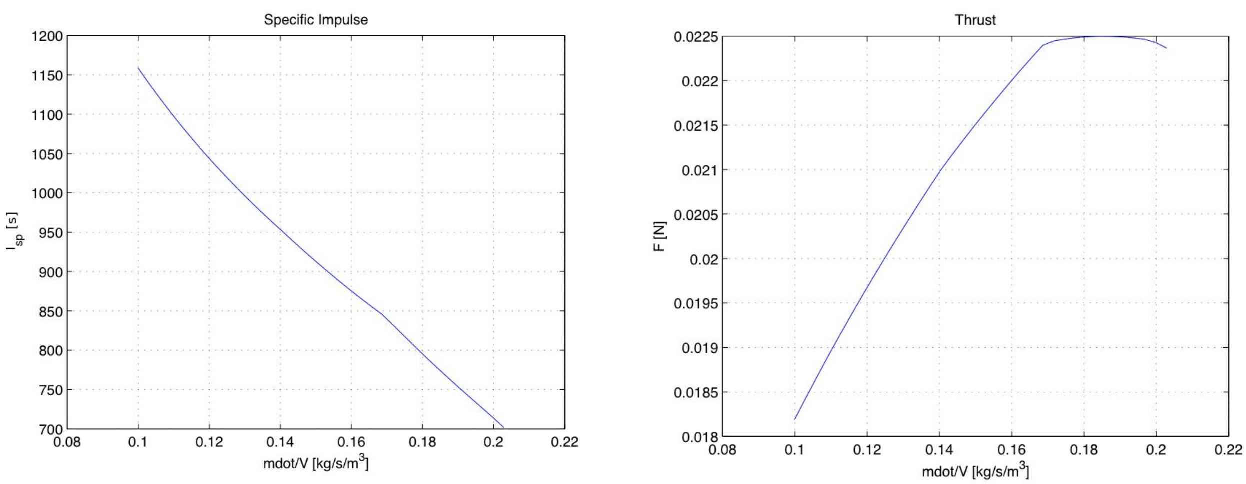

Figure 5 - Specific impulse and thrust versus mass flow rate normalized by the source volume.

Figure 6 shows that an increase in mass flow rate causes a reduction of the ionization fraction, which is the ratio between residual neutral density and electron density. Additionally, input power is lost at the wall at higher mass flow rates. After preliminary sizing of the thruster, we estimate the power to be dissipated by the radiator conservatively as the difference between the total power and the jet power, which is 1100 W.

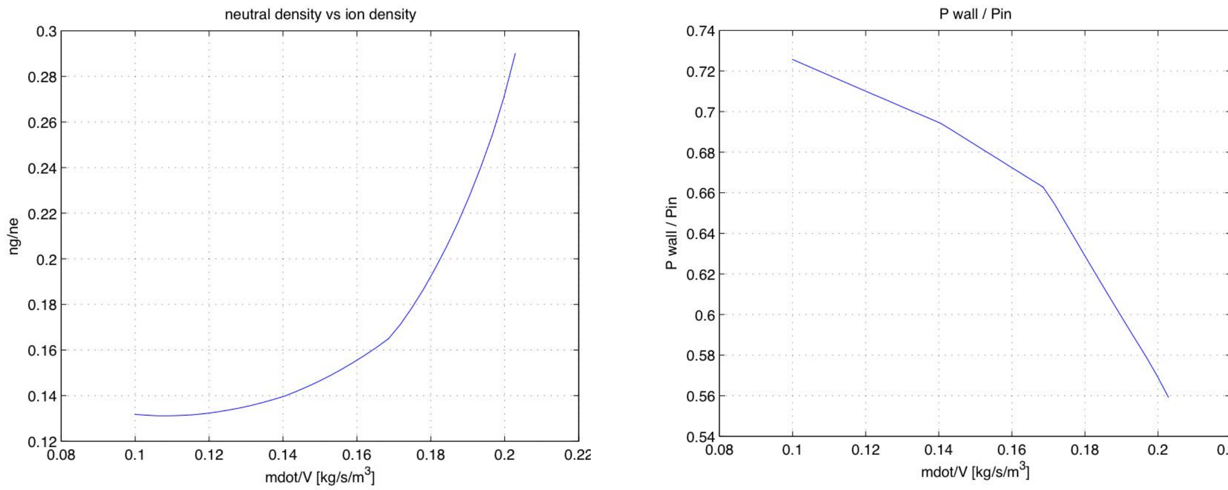

Figure 6 – (Left) The ratio of ion density to residual neutral density, and (Right) the ratio of power loss at the wall to applied external power versus mass flow rate normalized by the source volume.

IV. Thruster preliminary design

Figure 7 shows a sketch of the thruster configuration used in the following analysis. The dielectric cylindrical wall has an external diameter of 35 mm and a length of 87 mm, and is attached to an interface plate which can be connected to the spacecraft. The helicon antenna is wrapped around the dielectric quartz tube. A metallic shell is placed around the antenna in order to support the insulating material and superconducting coils with its support/cooling element. The superconducting coil is utilized in order to save mass and volume.[44] The main superconductor features from which enormous benefits on board spacecraft are:

- ability to carry high current densities which leads to substantial coil weight and dimensions reduction;
- at critical temperature electrical resistivity decreases to an immeasurable value: it means that ohmic heating of the magnet coil drops to zero, *i.e.*, no electrical power is wasted. Superconductivity at low temperature requires liquid helium at 4.2 K to produce very high current densities: the thermal analysis shows that high temperature superconductors are preferable because these can support lower current densities, but with a higher critical superconductivity temperature (>77 K), easier to maintain during the whole mission. The material chosen is a BSCCO (Bismuth Strontium Calcium Copper Oxide) high temperature superconductor. The use of permanent magnets is considered, however; the generated magnetic field is normally very non-uniform, with reversal regions and null points (cusps).[45] The strong non-uniformity can impede wave propagation and plasma flow, and eliminate the effects of enhanced plasma production and potential drop formation. Thus, accurate numerical model and experimental investigation need to be carried out prior to proceeding with a detailed thruster design based on this technology. In this research work attention is focused only on superconductor option because of the lower uncertainty of design associated to this solution.

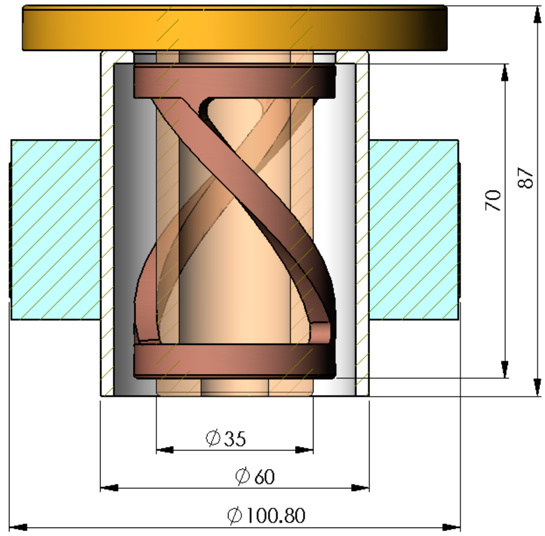

Figure 7 - Schematic of plasma thruster (Units: mm)

A. Thermal analysis

A sensitivity study is performed on a simplified thermal model of the thruster. Figure 8 presents a schematic view of the plasma thruster considered for the steady-state thermal analysis. The model is implemented using Esarad & Esatan software.

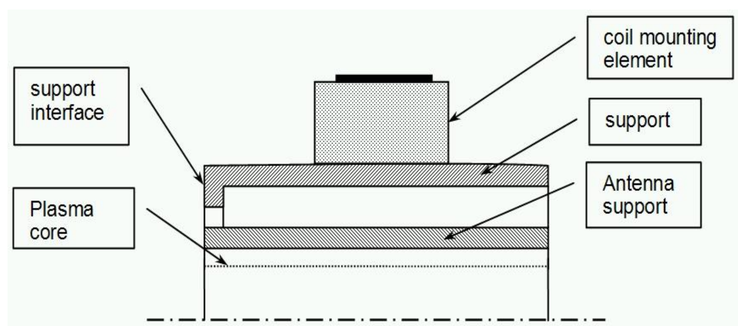

Figure 8 – Cross section of plasma thruster

The parameters considered for the sensitivity study ares: (i) boundary support interface temperature, (ii) boundary radiative external environment temperature, (iii) support interface material conductivity (S/C interface temperature), and (iv) the plasma power. The temperature reached in the different parts of the thruster and the expected thermal fluxes for each case are evaluated. The material considered for the main parts are: fused quartz for antenna support, aluminum alloy (thermal conductivity 170 W/(m·K)) or titanium alloy (thermal conductivity 7 W/(m·K)) for the support.

Figure 9 shows the mean temperature obtained for different temperatures of the boundary support interface (at the S/C interface) when the support is constructed of aluminum alloy. The maximum service temperature for these alloys is 250-280 °C, a reasonable upper limit for the boundary temperature interface is 50 °C. The temperature evaluated for the antenna support represents a worst case estimation, in fact in the model this part is considered conductively thermal decoupled from the support interface, in any case the temperature reached is compatible with the max continuous temperature for the fused quartz, 1000 °C, further detailed model that implement also the low conductive link for the antenna support with the support interface will allow to reduce a little bit its mean temperature. The results in any case highlight that the thermal flux generated by the plasma in this configuration should be removed from the support interface for the 75% and only a 25% is exchanged radiatively with the external environment this is due to the reduced dimensions of the system and the relatively low temperature of support part.

The thermal flux at support boundary interface can be moved at the spacecraft radiator with dedicated heat pipes. Assuming a spacecraft radiator with the dimensions of 1350 mm x 1350 mm, temperature of 40 °C, and a emissivity ε=0.8 the dissipated thermal flux is about 800 W.

Boundary Support Interface Temperature (C)	Support Mean Temperature (C)	Antenna Support Mean Temperature (C)
-20	185	968
-10	194	968
0	204	968
10	213	969
20	222	969
80	277	972
150	340	976

Radiative environment temperature = -10 °C
Conductive thermal flux at support interface = ~ 530 W
Radiative thermal flux at support interface = ~ 220 W
Radiative thermal flux at external environment = ~ 250 W

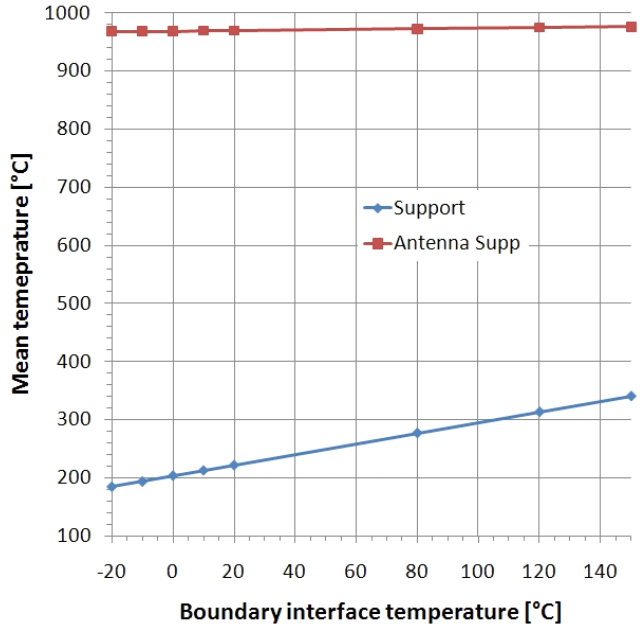

Figure 9 - Effect of S/C interface temperature; support realized with thermally conductive material (e.g. Aluminum alloy)

Analysis is also done using: (i) titanium alloy (Ti 6Al 4V) for the support, (ii) support boundary temperature of 20 °C and a (iii) radiative environment temperature of -10°C. The results show that the exchanged flux with the support boundary interface is reduced (thermal flux ~400 W) while the radiative flux exchanged with the environment is increased (~600 W). This leads to a higher temperature for different parts of the system: the support and the antenna support reached 750 °C and 1050 °C, respectively. The high temperature of the support requires more effort to thermally decouple the coil element from the support, but in any case the S/C radiator area could be reduced. Further analysis will be performed in order to asses a trade off for the required resources at system level.

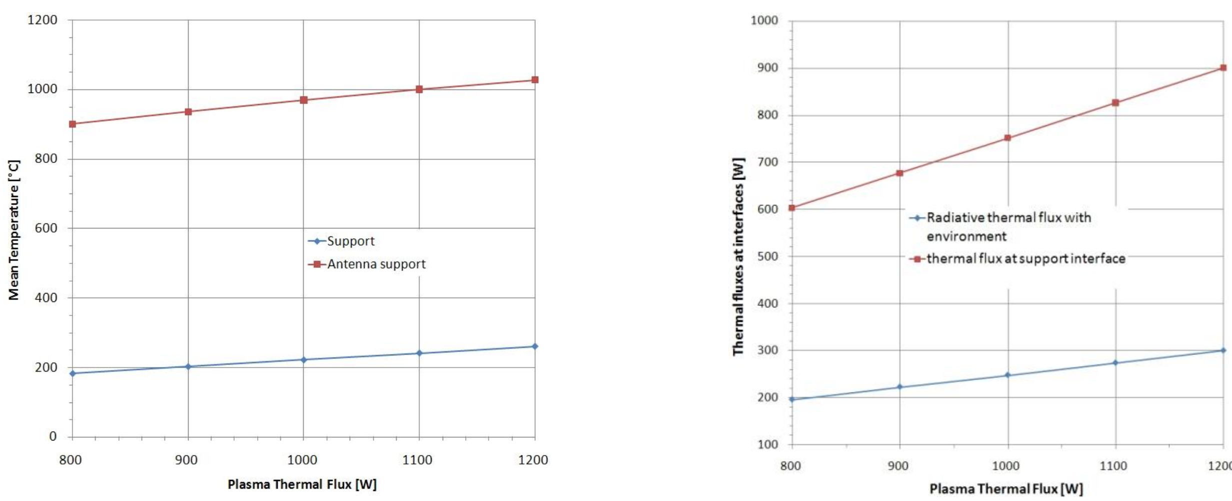

Figure 10 – (Left) support and antenna support temperature versus thermal plasma dissipate power. (Right) Thermal fluxes at each interface; (support boundary temperature = 20 °C, radiative environment = -10 °C)

Figure 10 shows the temperature of the support and antenna support in addition to the thermal fluxes at each interface with reference to the configuration: (i) aluminum alloy support, (ii) support boundary temperature of 20 °C, (iii) a radiative environment temperature of -10 °C, and (iv) a dissipated thermal power from the plasma between 800-1200 W. An increase of 100 W on thermal plasma flux means a mean increase on support temperature of 20 °C and of 30 °C on antenna support. The ratio of thermal fluxes at interfaces versus the plasma thermal flux does not change significantly in the range considered. Further analysis and a more detailed model will be performed in order to evaluate the antenna support temperature and the antenna temperature versus its electrical resistivity considering different mounting configuration.

The use of superconductor tapes for the generation of the required magnetic field makes it possible to save mass, volume and power. On the other side, the thermal control of superconductor materials is a critical issue because they require very low operating temperatures. The material chosen is BSCCO (Bismuth Strontium Calcium Copper Oxide), which is a high temperature superconductor with a critical temperature of 105 K. Therefore, the operating temperature is set to 40 K, accounting for a safety margin.

In the previous simulation, considering the coil mounting element realized with silica aerogel to thermally decouple the parts from the support, the expected thermal flux that should be removed from coil at temperature of 40 K is about 8.5 W with aluminum support or 18 W with titanium support. To remove this thermal flux there are some possible solutions with different system impact and that should be evaluated after a trade off process. The first possibility (in the case of aluminum support) should be removed the thermal flux from low temperature coil with a dedicate cryocooler the second possibility is to removed a fraction of this flux with a dedicate radiator in order to have a lower part of flux that should be removed from the coil at low temperature with a minor resources demanding cryocooler. For example, with reference to Figure 4 for an aluminum support, if a dedicated radiator (ε=0.8) is foreseen to have an intermediate temperature of -20 °C the flux at the radiator should be about 4.8 W (coil part removes about 3.7 W) and its minimal dimensions should be 190 mm x 190 mm.

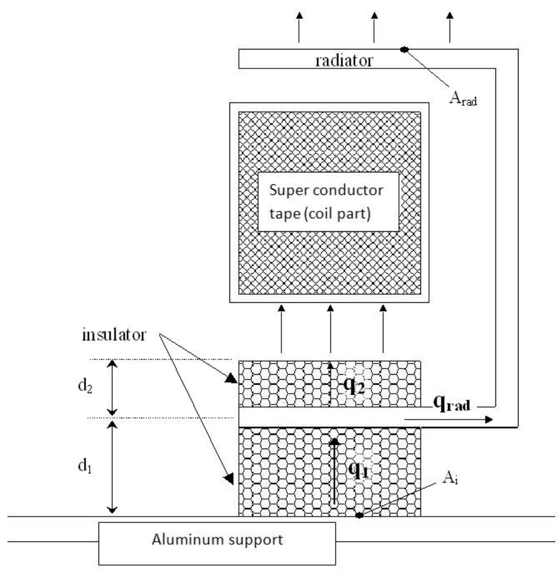

Figure 11 - Possible architecture to reduce the thermal flux at coil part

B. Mechanical analysis

For the previous thruster scheme a finite element model is developed with MSC-Nastran software to evaluate the Eigen frequencies of the system and the stress level in the main components at quasi static loads. The model is realized with plate elements, the materials considered for the support is aluminum alloy (7075-T6) while fused quartz is used for the antenna support. The mass of helicon is locally distributed on to the antenna support. The mass of coil and coil mounting element are locally distributed on the support part. The connection between the quartz and the interface plate is disk of inconel for the dynamic and static evaluation. **Error! Reference source not found.** shows the mass breakdown of the main components.

Table 2 – Mass breakdown of thruster.

Part	Mass [g]
Support	120
Antenna support	75
Coil mounting element	90
Helicon	125
Total	**410**

The model in Figure 12 is composed of 2569 elements and 2526 nodes. Two type of analysis are carried out, the normal modes and the static one. The first evaluation is aimed to verify that the Eigen frequency of the structure is higher of 150 Hz (value referred to the payload mounted on a S/C) while the second analysis considers a quasi static load applied spherically (in case of Arianne 5 launcher at the S/C primary interfaces for a payload with a mass lower of 1 kg the quasi static acceleration is 700 m/s^2).

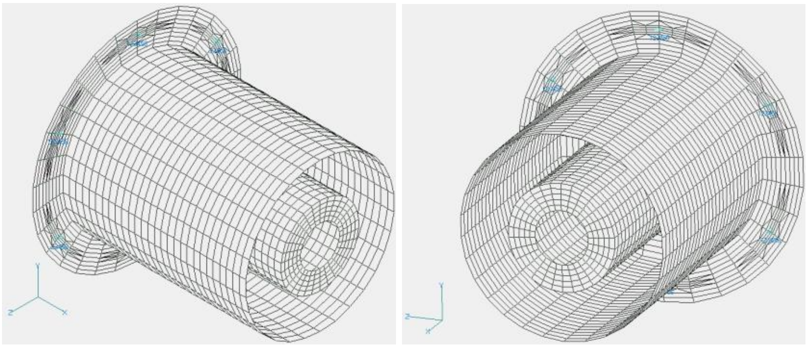

Figure 12 - Finite element model of the thruster.

Some results are reported in the following images, the first Eigen frequency is 885 Hz, with flexional mode shape, the max displacement at the quasi static loads is 0.06 mm while the max stress (Von Mises criteria) for the support part is about 25 MPa and for the antenna support component is 6 MPa.

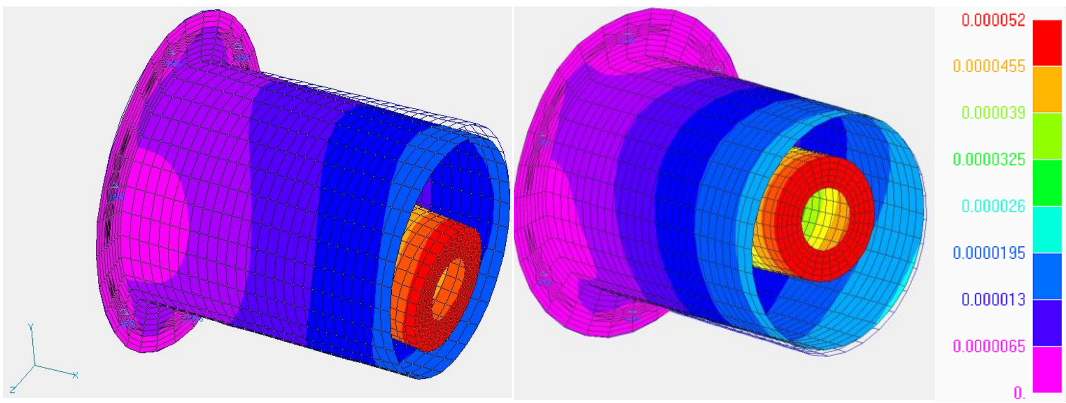

Figure 13 – (Left) The first Eigen-mode of the system. (Right) The displacement at quasi static load acting spherically along the positive axis directions.

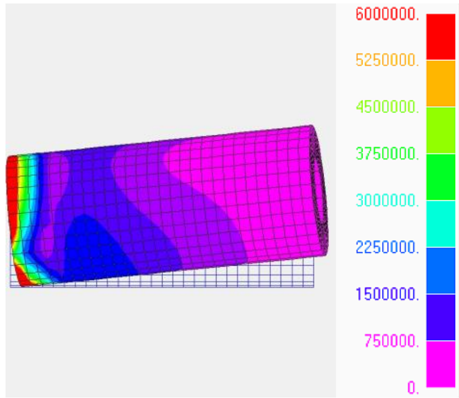

Figure 14 - Max stress (Pa) evaluated with Von Mises criteria for the antenna support component with the quasi static loads.

In all cases, the results fulfill the requirements for the structural feasibility study, additional detailed thermoelastic analysis should be carried out to refine the interface between support and antenna support to accommodate the different CTE materials and reduce the local stress concentration.

V. Conclusion

A preliminary design of a medium-power helicon plasma thruster is conducted through: (i) analysis and optimization of the plasma section, and (ii) preliminary thermo-mechanical analysis and design. The magnetic section is sized considering superconductor technology, which has a strong impact at the system level. Permanent magnets provide a more efficient solution, however due to irregularities in the magnetic field space-configuration, This solution requires further analysis with a 3-D code that has yet to be developed, as well as a dedicated test campaign. Preliminary analysis shows that the structural mass of the thruster can be less than 1 kg, which excludes the mass of RF power unit, magnetic field control unit, and other subsystem components.

References

[1]Pavarin, D., "Diagnostic and optimization procedures for gas and plasma propulsion system", Ph.D. Thesis, University of Padua, 2001.

[2]Goulding, R. H, Pavarin D, Angrilli F, Barber GC, Carter MD, Maggiora R, Sparks DO, "Helicon plasma source configuration analysis by means of density measurements" ICEAA, Torino, Italy, 1999.

[3]Rocca S, "Design and modeling of an experiment for the performance evaluation of a variable specific impulse magnetoplasmadynamic thruster", PhD thesis in Mechanical Measurements for Engineering, University of Padua, 2005.

[4]Goulding, R. H, Baity, F. W., Barber, G. C, Carter, M. D., Chang-Díaz, F. R., Pavarin, D., Sparks, D. O., Squire, J. P., "Helicon plasma source optimization studies for VASIMR," APS Meeting, 1999.

[5]Suwon C, "A self consistent global model of neutral gas depletion in pulsed helicon plasmas," Physics of Plasmas, Vol. 6, Jan 1996, pp. 359-365.

[6]Gilland J, "Neutral Pumping in a Helicon Discharge," Plasma Sources Sci. Tech., Vol. 7, 1998, pp. 416-422.

[7]Zorat, R., "Global model of a radio frequency H2 plasma in DENISE", Plasma Sources Sci Tech, Vol. 9, 2000, pp. 161-168.

[8]Chung TH, "Global model and scaling laws for inductively coupled oxygen discharge plasmas" J. Appl. Phys. Vol. 86, No. 7, Oct, 1999.

[9]Lee, C., "Global Model of Plasma Chemistry in a High Density Oxygen Discharge," J. Electrochem. Soc, Vol. 141, No. 6, June 1994.

[10]Cheetham AD, "Characterization and modeling of a helicon plasma source," J. Vac. Sci. Tech. A Vol. 16, No. 5, Sep-Oct 1998.

[11]Lieberman, M. A, "Global Model of pulse-power-modulate high-density, low-pressure discharges," Plasma Sources Sci. Tech. Vol. 5, 1996, pp. 145-158.

[12]Lee, C., "Global Model of Plasma Chemistry in a High Density Oxygen Discharge," J. Electrochem. Soc, Vol. 141, No. 6, June 1994.

[13]Ashida, S., "Spatially averaged (Global) model of time Modulated High Density Chlorine Plasmas," J. Appl. Phys., Vol. 36, 1997, pp. 854-861.

[14]Ashida, S., "Spatially averaged (global) model of time modulated high density argon plasmas," J. Vac. Sci. Tech. A, Vol. 13, No. 5, Sep/Oct, 1995.
[15]Meyyappan, M., "A spatially-averaged model for high density discharges," Vacuum, Vol. 47, No. 3, 1996, pp. 215-220.
[16]Gordies, B., "Self-consistent kinetic model of low-pressure N2-H2 flowing discharges I-II," Plasma sources Sci. Tech, Vol. 7, 1998, pp. 378-388.
[17]Lee, C., "Global model of Ar, O2, Cl2, and Ar/O2 high-high density plasma discharges," J. Vac. Sci. Tech. A, Vol. 13, No. 2, Mar/Apr, 1995.
[18]Nakano, T., "Ion and neutral temperature in electron cyclotron resonance plasma reactors", Appl. Phys. Lett., Vol. 58, No. 5, 1991, pp. 458-460.
[19]Hopwood, J., "Neutral gas temperature in a multipolar electron cyclotron resonance plasmas," Appl. Phys. Lett., Vol. 58, No. 22, June, 1991.
[20]Milora, S. L., "Quickgun: an algorithm for estimating the performance of two-stage light gas guns" ORNL/TM-11561 report.
[21]Mitchner, M., "Partially Ionized Gases," A. Willy, 1973, New York.
[22]McDaniel, E. W., *Collision Phenomena in Ionized Gases*, John Willey & Sons, New York, 1964.
[23]Janev, R. K., "Elementary processing hydrogen helium plasmas," Springer-Verlag, 1987.
[24]Barnet, C. F., "Collision of H, H2, He and Li atoms and ions with atoms and molecules," ORNL
[25]Godyak, V. A.: *Soviet Radio Frequency Discharge Research* (Falls Church VA: Delphic Associates, 1986).
[26]Mozetic, M., "Atomic hydrogen density along continuously pumped glass tube," Vacuum, Vol. 5, No. 3-4, 1998, pp. 319-322.
[27]Tynan, G. R., "Neutral depletion and transport mechanism in large-area high density plasma sources," Journal of Applied Physics, Vol. 86, No. 10, Nov. 1999.
[28]Lieberman, M. A, "Principles of Plasma Discharges and Material Processing", New York Wiley, 1994.
[29]Lee, C., "Global Model of Plasma Chemistry in a High Density Oxygen Discharge," J. Electrochem. Soc, Vol.141, No. 6, June 1994.
[30]Dushmann, S., *Scientific Foundations of Vacuum Technique*, 4th Ed., John Wiley & Sons Inc., New York, 1964.
[31]Holland, J., Steckelmacher, W., Yarwood, J. "Vacuum Manual," Halsted Press, (division of J Wiley and Sons), New York, 1974.
[32]Chapman, "The mathematical theory of non uniform gas," Cambridge At the University Press, 1970.
[33]Panevsky, M. I., "Characterization of the Resonant Electromagnetic Mode in Helicon Discharges," Ph.D. Thesis, University of Texas at Austin, 2003.
[34]Verboncoeur, J. P., Langdon, A. B., Gladd, N. T., "An Object -Oriented Electromagnetic PIC Code," Comp. Phys. Comm., 87, May 11, 1995, pp. 199-211.
[35]Birdsall, C., Langdon A., "Plasma Physics via computer simulation," IoP, Bristol, 1991
[36]Raadu, A., "Particle Acceleration Mechanisms in Space Plasmas", Phys. Chem. Earth (C), Vol. 26, No. 1, 2001, pp.55-59.
[37]Raadu, A., "The physics of double layers and their role in astrophysics," Physics Reports, Vol. 178, No. 2, 1989, pp. 25-97.
[38]Perkins, Sun, Y. C., "Double Layers without current," Phys. Rev. Lett., Vol. 46, 1981, pp. 115.
[39]Chan, M., Cho, H., Hershkowitz, N., Intrator, T., "Experimental observation of slow ion acoustic Double Layers" Phys. Rev. Lett., Vol. 57, 1986, pp. 3050-3053.
[40]Charles, C., Boswell, R. W., "Laboratory evidence of a supersonic ion beam generated by a current-free "helicon" doublelayer," Physics of Plasmas, Vol. 11, 2004, pp. 1706-1714.
[41]Charles, C., "Hydrogen ion beam generated by a current-free double- layer in a helicon plasma," Applied Physics Letters, Vol. 84, 2004, pp. 332-334.
[42]Charles, C., Boswell, R. W., "Current-free double-layer formation in a high -density helicon discharge," Applied Physics Letters, Vol. 82, 2003, pp. 1356-1358.
[43]Manente, M., Carlsson, J., Musso, I., Bramanti, C., Pavarin, D., and Angrilli, F., "Numerical simulation of the Helicon Double Layer Thruster Concept," IAAA-2007-5312, 43rd AIAA/ASME/SAE/ASEE Joint Propulsion Conference, Cincinnati, OH, 2007.
[44]Bruno, C., Giucci, S., "Cryogenic technology to improve electric thrusters," Acta Astronautica, Vol. 51, No. 12, pp. 855-863, 2002.
[45]Shamrai, K. P., Virko, Y. V. , Virko, V. F., Yakimenko, A. I., "Compact Helicon Plasma Source with Permanent Magnets for Electric Propulsion Application," AIAA-2006-4845, 42nd AIAA/ASME/SAE/ASEE Joint Propulsion Conference & Exhibit, Sacramento, CA, July 9–12, 2006.